Pro5 is not essential for the formation of 'Ni-hook' in nickel superoxide dismutase

Pro5 is not essential for the formation of 'Ni-Hook' in Nickel Superoxide Dismutase

Priyanka Basak[1], Barbara Zambelli[2], Diane E. Cabelli[3], Stefano Ciurli[2], Michael J. Maroney[1,4*]

[1]Department of Chemistry, University of Massachusetts Amherst MA 01003, USA

[2]Laboratory of Bioinorganic Chemistry, Department of Pharmacy and Biotechnology, University of Bologna, Italy

[3]Department of Chemistry, Building 555A, Brookhaven National Laboratory, P.O. Box 5000, Upton, New York 11973, USA

[4]Program in Molecular and Cellular Biology, University of Massachusetts, Amherst, MA 01003, USA

*Corresponding Author

Abstract

The N-terminus of nickel-dependent superoxide dismutase (NiSOD), forms a structural motif known as the "Ni-hook," where the peptide wraps around the metal to bring cysteine-2 and cysteine-6 into spatial proximity, allowing these residues to coordinate in a *cis*-geometry. A highly conserved proline-5 residue in the Ni-hook adopts a *cis*-conformation that is widely considered important for its formation. Herein, we investigate this role by point mutation of Pro5 to alanine. The results obtained show that the variant exhibits wild-type-like redox catalysis and features a Ni(III) center very similar to that found in enzyme. Structural analysis using x-ray absorption spectroscopy of the nickel sites in as-isolated P5A-NiSOD reveals changes in the variant and are consistent with a six-coordinate Ni site with $(N/O)_4S_2$ coordination. These changes are attributed to changes in the Ni(II) site structure. Nickel-binding studies using

isothermal titration calorimetry reveal two binding events with k_d = 25(20) nM, and 250(60) nM. These events are attributed to i) Ni(II) binding to a preformed Ni-hook containing *cis*-Pro5 and ii) the combination of *trans*- to *cis*- isomerization upon Ni(II) binding, respectively. The higher-affinity binding event is absent in P5A-NiSOD, an observation attributed to the low abundance of the *cis*-Ala5 isomer in the apo-protein.

Key Words

NiSOD, Ni-Hook, *cis-/trans* isomerization, isothermal titration calorimetry, x-ray absorption spectroscopy

Abbreviations

EXAFS, extended x-ray absorption fine structure; ITC, Isothermal titration calorimetry; NiSOD, nickel-dependent superoxide dismutase, LMCT, ligand-to-metal charge transfer; XANES, x-ray absorption near-edge structure; XAS, x-ray absorption spectroscopy.

1. Introduction

Superoxide dismutases are enzymes that catalyze the disproportionation of toxic superoxide radical to oxygen and hydrogen peroxide employing a ping-pong mechanism. Such a mechanism requires a metal that oscillates between two redox states separated by one electron (*e.g.,* Cu(I/II), Mn(II/III) and Fe(II/III) with an optimum potential of ~300 mV to alternately oxidize and reduce superoxide[1]. Nickel-dependent superoxide dismutase (NiSOD) is a distinct representative of the SOD family of metalloenzymes that features a homohexameric quaternary structure and employs a unique nickel active site for catalysis[1, 2]. Because Ni(II) ions have no redox chemistry in aqueous solution, the enzyme relies on the protein environment to stabilize the Ni(II/III) couple to make it accessible for catalysis. The NiSOD active site is located at the N-terminus of each subunit, in which the highly conserved N-terminal HCXX**P**CXXY sequence forms the 'Ni-hook' motif **(Figure 1)** that is disordered in absence of nickel[3, 4]. The nickel center in the holo-enzyme is coordinated in a planar fashion by the N-terminal amine (His1), the Cys2 backbone amidate N atom, and two thiolates from Cys2

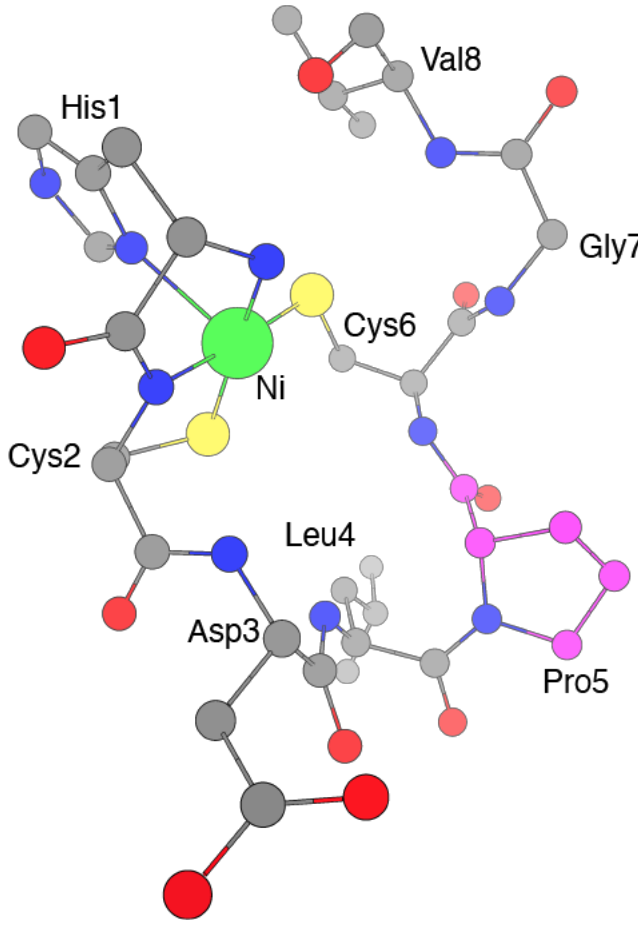

Figure 1. Ball & Stick representation of residues 1 – 8 (HCDLPCGV) of Ni-hook in as-isolated WT-NiSOD (PDB ID: 1T6U). His1 is shown in the His_{on} configuration observed in Ni(III). Side chain of *cis*-Pro5 is shown in magenta.

and Cys6 in *cis*-geometry[3-5]. An additional δ-N- ligand from the imidazole of His1 binds axially to the Ni(III) site[3, 4]. This unique combination of ligands adjusts the redox potential of the Ni(II/III) couple to the requisite potential (290 mV) for SOD catalysis and results in the aerobic isolation of the enzyme as a ~50:50 mixture of Ni(II) and Ni(III)[6].

In addition to containing all the Ni ligands, the Ni-hook motif contains a Pro5 residue that is conserved in all known examples of NiSOD with the exception of two from *Mycobacterium sp.,* where the Pro residue is substituted by Tyr or Phe[7]. Crystallography shows that this Pro residue adopts a *cis* conformation in the holo-enzyme that appears to be crucial for positioning Cys6 in spatial proximity to Cys2 in the Ni site, resulting in *cis*-coordination of the two thiolates in the complex **(Figure 1)**[4, 8]. In folded proteins, while the non-prolyl peptide bonds exist predominantly in *trans*- conformation, the prolyl peptide bond can readily populate either *trans*- or *cis*- conformations. In unfolded proteins, the Xaa-Pro peptide bond occurs as an equilibrium mixture of both *cis*- (~20-30%) and *trans*- isomer (~70-80%)[9, 10]. In the case of NiSOD, it is easy to envision a model for the formation of the Ni-hook wherein Ni binds to the *cis*-Pro5 isomer, trapping the Ni hook, and by Le Chatelier's principle ends up producing exclusively the *cis*-Pro5 isomer in the complex. Recent support for this view has been obtained from a Pro5 to Ala variant of a NiSOD model peptide[11].

In this study, we report on production and characterization of a P5A-NiSOD variant. Unexpectedly, the variant has WT-like SOD activity and spectral properties that indicate that Pro5 does not play a critical role in the formation of the Ni-hook. Given the requirement for *cis*-coordination of Cys2 and Cys6, this result suggests that the formation of the NiSOD active site complex is sufficient to induce trans → cis isomerization of Ala in the P5A variant or trap the trace amount of *cis*-Ala5 that forms spontaneously.

2. Materials and Methods

2.1 Protein Samples

P5A-NiSOD was produced by single point mutation of a *S. coelicolor* NiSOD gene construct that incorporates a pelB leader sequence that allows for N-terminal processing and isolation from the periplasmic space of *E. coli cells*, as previously described[4]. Briefly, a pET-22b (+) vector (with Ampicillin resistance) encoding the wild-type *S. coelicolor* NiSOD sequence preceded by a pelB sequence was used as the template DNA for the single point mutation using polymerase chain reaction (PCR) with the following primers: forward - 5' GACCTGGCCTGCGGCGTGTAC 3', and reverse - 5' GTACACGCCGCAGGCCAGGTC 3'. These primers were designed to incorporate the desired Pro5 to Ala mutation (indicated by the underline). For each 50 μL volume of PCR reaction mixture, 0.5 μM of each primer was used for 2 ng of template DNA. Successful PCR amplifications were determined using an 0.8% agarose gel, and the amplicons were subsequently digested with DpnI for 1 hour at 37 ^{o}C to remove any methylated template DNA. The digested PCR mixture was then used to transform DH5α competent cells. The transformed cells were grown in 0.5 mL Luria Bertini (LB) media in 5 ml tubes at 37 °C for 1 hour and aliquots were plated on agar plates containing ampicillin antibiotic followed by a 12–16-hour incubation at 37 °C. Single colonies were grown to saturation in 5ml LB-miller broth supplemented with ampicillin at 37 ^{o}C. Cells were pelleted at 13, 000 g for 5 minutes and the plasmids were isolated using GeneJET plasmid miniprep kit (Thermo Fisher Scientific). Gene sequencing (Genewiz, Inc.) confirmed the successful mutation.

The pET-22b-pelB-P5ANiSOD plasmid construct was used to transform BL21(DE3) cells. The transformed cells were grown in 0.5 mL Luria Bertini (LB) media in 5 ml tubes at 37 °C for 1 hour and aliquots were plated on agar plates containing ampicillin antibiotic followed by a 12–

14-hour incubation at 37 °C. A single colony was picked and grown overnight in LB media (200 mL) supplemented with ampicillin at 37 °C with shaking at 200 rpm. A 10 mL aliquot of the overnight culture was added to 1 L of the pre-warmed fresh LB media containing ampicillin, grown to an OD_{600} of 0.6 - 0.8, and then induced with 0.8 mM of isopropyl – β-D-1-thiogalactopyranoside for 3 - 4 hours at 37 °C. Cells were harvested by centrifugation at 4, 000 g for 15 min and then re-suspended in 100 mL of osmotic shock buffer (20% sucrose, 1 mM EDTA, 30 mM Tris•HCl, pH 8.0) per liter of culture. The cell suspension was shaken at 180 rpm for 15 minutes at room temperature and centrifuged at 4, 000 g for 10 minutes. The supernatant was discarded, and the cells were then re-suspended in 100 mL ice-cold 5 mM $MgSO_4$ per liter of culture. The resuspended cells were shaken at 4 °C for 10 minutes and then centrifuged at 10, 000 g for 10 minutes. The pellet was discarded, and the supernatant was collected for further purification.

All chromatographic purification steps were carried out using AKTA-FPLC system (Amersham Biosciences). The supernatant was loaded onto a pre-equilibrated Q-Sepharose column (GE Health Sciences) at a rate of 2.00 ml/min with Buffer A (50 mM Tris, pH 8.0). Once the absorbance returned to baseline value, the protein was eluted with a linear gradient of Buffer B (50 mM Tris, 1 M NaCl, pH 8.0). All the fractions containing protein was collected and analyzed using SDS-PAGE. Fractions containing P5A-NiSOD (MW 13, 174 Da) were pooled and loaded on a 120 mL HiLoad 16/60 Superdex 75 (GE Life Sciences) column equilibrated with Buffer C (50 mM Tris, 200 mM NaCl, pH 8.0). Protein fractions were collected based on the absorbance values at 280 nm and the purity of collected protein fractions were analyzed by SDS-PAGE (**Figure SI-1A**). Fractions containing P5A-NiSOD were pooled, concentrated and frozen at -20 °C until ready to use. The molecular weight of the purified protein was confirmed using electrospray - ionization mass spectrometry (ESI-MS) on a denatured sample in 1:1 Methanol/water mixture

on a Thermo Orbitrap Fusion Tribrid instrument. The molecular weight of apo-P5A-NiSOD was calculated as 13,174.9 Da, found 13, 171.1 Da (**Figure SI-1B**).

Samples of holo-P5A-NiSOD for spectroscopic characterization and activity assays were obtained by metalating the apo-protein with $NiCl_2$. All metalation steps on the purified apo-P5A-NiSOD protein were performed inside an anaerobic glovebox (0-10 ppm O_2 and 3% H_2; Coy Laboratory Products, Inc.). The purified apo-proteins were reduced with 5-fold excess of DTT (Dithiothreitol), and excess DTT was removed by buffer exchanging the protein with degassed Buffer C (50 mM Tris, 200 mM NaCl, pH 8.0) using spin columns (Amicon, 3 kDa MWCO). The reduced and buffer-exchanged protein was then metalated by adding 3-fold excess of aqueous $NiCl_2$ stock solution (9.34 mM) and incubating for 2 hours. Excess nickel was removed by adding Chelex beads (Sigma Aldrich) to the sample, which was then incubated for 30 minutes at room temperature. Aliquots of this sample were then buffer exchanged into the buffers used for each technique: Buffer C (*vide supra*) for UV-vis and EPR, Buffer X (50 mM Tris, 200 mM NaBr, pH 8.0) for XAS, and 10 mM phosphate, 30 mM formate, 5 μM EDTA, pH 7.5, for enzyme assay, using centrifugal filters (Amicon, 3kDa MWCO).

ICP-MS was used to quantify the nickel content of each of the holo-P5A-NiSOD samples, except where noted. Briefly, a 5 μL aliquot from each sample was diluted to 0.5 mL, which was then mixed with 0.25 mL of aqua-regia, and the final volume was adjusted to 5 mL. The samples were injected into ICP-MS (Perkin Elmer Nexion) and the nickel content of the sample was determined using the standard calibration curve which was made from standard solutions containing nickel from 0 ppb - 40 ppb. Each of the standard solution (5 mL each) was prepared from a 100 ppb stock solution that was prepared using an aliquot of ICP-MS standard QC 21

(Analytical West). Deionized water was used as the blank, and the intensity of ^{58}Ni obtained from the blank was subtracted from each reading.

SOD activity assays were performed at the Van de Graaf generator located at the ACER facility at Brookhaven National Laboratory. Catalytic rate constants were obtained by monitoring the disappearance of pulse-radiolytically produced O_2^- at 260 nm in buffer solutions (10 mM phosphate, 30 mM formate, and 5 μM EDTA, pH 7.5) in the presence and absence of as-isolated P5A-NiSOD using a previously published procedure[12]. The sample of P5A-NiSOD was determined to contain 0.434 μM Ni by ICP-MS.

2.2 Spectroscopic Characterizations

2.2.1 Electronic Absorption Spectroscopy

UV-vis spectra were obtained on a Hewlett-Packard 8453 spectrophotometer and used to determine the protein concentrations for each experiment and characterize the spectra of 'as-isolated' P5A-NiSOD and reduced P5A-NiSOD. Protein concentrations for apo- and holo-protein monomers were determined using a molar extinction coefficient of 17080 $M^{-1}cm^{-1}$ at 280 nm that was calculated from the amino acid content using the Expasy Webserver. This value is comparable to an experimentally determined value of ~17000 $M^{-1}cm^{-1}$ calculated for the as-isolated monomer protein from data in the literature[13]. For apo- protein samples, spectra were obtained on samples of P5A-NiSOD diluted to 100 μM in monomer with Buffer C while for holo-as-isolated samples, spectra were obtained on samples of WT- or P5A-NiSOD diluted to 100 μM in nickel concentration with Buffer C.

2.2.2 Electron Paramagnetic Resonance (EPR) Spectroscopy

X-band EPR spectra of as-isolated holo-P5A-NiSOD were collected at 77 K using a finger dewar on a Bruker Elexsys E-500 EPR instrument equipped with DM4116 cavity at 9.609 GHz frequency, 6.0131 mW power, 10 G modulation amplitude, 100 GHz modulation frequency, and a 327 ms time constant. A 200 µL aliquot of a solution of as-isolated holo-P5A-NiSOD (0.3 mM based on nickel concentration determined by ICP-MS described above) was transferred to EPR tubes and frozen in liquid nitrogen which was then used for EPR experiments. Processing (spectral smoothening and baseline correction) was performed using the in-built the Xepr program. Spin integration of the EPR signal from as-isolated holo-P5A-NiSOD was performed by comparing the double integration of the first derivative signal vs. a Cu(II) standard (0.283 mM $CuSO_4$ in 2 M $NaClO_4$ and 10 mM HCl), where the Cu content was determined by ICP-MS, as described above.

2.2.3 X-ray Absorption Spectroscopy (XAS)

X-ray absorption spectral data were obtained on sample of P5A-NiSOD prepared as described above and then concentrated to 100 µl using centrifugal filters (Amicon, 3kDa MWCO). An aliquot from this sample was used to determine the nickel content using ICP-MS (1.52 mM), and protein concentration was determined using UV-vis absorbance. The ratio of nickel:P5A-NiSOD protein was 0.85. The remaining sample was then mixed with glycerol to 11% by volume and loaded into kapton-taped polycarbonate holders and then rapidly frozen in liquid nitrogen.

Ni K-edge XAS data were collected in remote operation mode on beamline 7-3 at the Stanford Sychrotron Radiation Laboratory (SSRL) using a Si(220) (in phi = 0° orientation) double crystal monochromator on samples held at 10 K in a liquid He cryostat (Oxford). Harmonic rejection was achieved by detuning the monochromator by 50%. X-ray absorption spectra were acquired in fluorescence using a 30-element Ge detector (Canberra) and the monochromator was

calibrated to the first inflection point of a Ni foil (8333.0 eV) by simultaneous collection of transmission data. The output of each channel was evaluated, and the resulting summed spectra were obtained from 29 channels. Data collection in the pre-edge baseline region (8130-8310) was collected in 10 eV steps with 1 s dwell time (19 points). Data in the edge and XANES regions (8310 – 8360 eV) were collected in 0.3 eV steps with 2 s dwell time (167 points) and data in the EXAFS region (1.6 k – 16.1 k) were collected in 0.05k steps, with dwell times increasing from 2 s to 9s in a k^2-weighted fashion.

Data reduction and analyses were performed according to a previously published procedure for Ni K-edge XAS data[12, 14-16]. The Sixpack software package[17] was used to process and normalize the XAS data. The XAS data shown for as-isolated P5A-NiSOD is an average of eight scans (for details, see Supporting Information).

2.3 Isothermal Titration Calorimetry Experiments

Ni(II) titrations were performed at 25 °C (apo-WT-SOD and apo-P5A-SOD) and at 35 °C (apo-WT-SOD), using a high-sensitivity VP-isothermal titration microcalorimeter (MicroCal LLC, Northampton, MA, USA). The reference cell was filled with deionized water. Stock proteins (apo-WT-SOD and apo-P5A-SOD) were thawed and incubated with 1-5 mM EDTA for two hours at room temperature, after which the samples were buffer exchanged in the reaction buffer (20 mM HEPES, 1 mM TCEP, 200 mM NaCl, pH 8.0). Protein and metal solutions were prepared by diluting concentrated stock solutions in the reaction buffer (20 mM HEPES, 1 mM TCEP, 200 mM NaCl, pH 8.0). To test for the role of Ni(II/III) oxidation in the ITC experiment, a buffer containing 10 mM Na_2SO_3 was used to prepare the protein and N(II) solutions. Each experiment started with a small injection of 1–2 μL, which was discarded from the analysis of the integrated data, in order to avoid artifacts due to the diffusion through the injection port occurring during the

long equilibration period, locally affecting the Ni(II) concentration near the syringe needle tip. Care was taken to start the first addition after baseline stability had been achieved. In each individual titration, 10 μL of a solution containing Ni(II) (150 μM or 500 μM) was injected into a solution of apo-WT-SOD (40 μM, concentration of the monomer) or apo-P5A-SOD (15 μM, concentration of the monomer), using a computer-controlled 310-μL microsyringe. All experiments were repeated at least three times to verify reproducibility and a control experiment was performed to verify that the heat of dilution was negligible. To allow the system to reach equilibrium, a spacing of 300 s was applied between each ligand injection. In order to obtain reproducible results, it was important to incubate the protein samples at the experimental temperature for 1.5 – 2 h prior to titration.

Integrated heat data, obtained for each titration using NITPIC[18] software, were fitted using a nonlinear least-squares minimization algorithm to a theoretical titration curve, using Origin software and one or two sets of sites models. N (stoichiometry), ΔH (reaction enthalpy change, kcal mol^{-1}) and K_a (binding constant) were the thermodynamic fitting parameters. The reaction entropy was calculated using the relationships $\Delta G = -RT\ln K_a$ (R = 1.987 cal mol−1 K−1, T = 298 K) and $\Delta G = \Delta H - T\Delta S$.

2.4 Computational Chemistry

The energetics of Ni binding to the pre-formed Ni-hook motif containing either *cis*-Pro5 or *cis*-Ala5, was evaluated using quantum mechanical calculations. The structure of the peptide that comprises the Ni-hook motif (the first 8 residues of Ni-SOD from *S. coelicolor*) and the bound Ni atom was taken from the PDB code 1T6U (chain A; all other chains of the dodecameric unit are superimposable). The conformation chosen for the side chain imidazole ring of His1 was that of the reduced enzyme, corresponding to the Ni(II) oxidation state of the

metal ion. In Spartan (v. Spartan18, Wavefunction Inc.), the positions of the H atoms were first optimized using simple molecular mechanics energy minimization, followed by an energy minimization using density functional at the wB97X-D/6-31G* level. In the case of the wild-type apo-protein, the initial model was built by removing the Ni atom and placing H atoms on the thiolate and amide functionalities, while for the Pro5-to-Ala5 mutant (P5A) the Cδ and Cε atoms of the proline residues were deleted, and the resulting valences substituted with H atoms prior to energy minimization as described above. In all calculations, the positions of the heavy atoms were left unchanged.

3. Results

3.1 Redox Catalysis

The P5A-NiSOD variant was found to have high SOD catalytic activity. The catalytic rate constant (k_{cat}) determined for as-isolated P5A-NiSOD using pulse-radiolytic generation of O_2^- and monitoring the disappearance of superoxide radical at 260 nm was 2.3 x 10^8 $M^{-1}s^{-1}$ at pH 7.5, which is 35% of the reported value of as-isolated recombinant WT-NiSOD (0.71 x 10^9 $M^{-1}s^{-1}$), where activity is reported on a per Ni basis.

3.2 Electronic Absorption Spectroscopy

The electronic absorption spectra of as-isolated P5A-NiSOD and as-isolated WT-NiSOD are compared in **Figure 2**. The spectrum of the variant is dominated by an intense transition at 370 nm (ε = 3000 $M^{-1}cm^{-1}$). Other than intensity differences, the spectra are very similar and consistent with the presence of very similar chromophores. The 370 nm transition in the spectrum of the as-

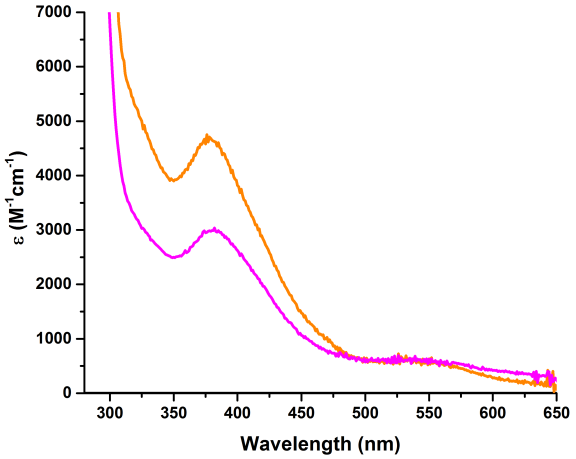

Figure 2. UV-Vis spectra of 100 μM (in total nickel concentration) as–isolated WT-NiSOD (orange) and as–isolated P5A-NiSOD (magenta).

isolated WT-NiSOD has been assigned to S → Ni(III) LMCT[19]. By analogy, the similarity of the two spectra are consistent with the presence of a WT-like Ni(III) site in P5A-NiSOD.

3.3 Electron Paramagnetic Resonance

The presence of a WT-like Ni(III) center in the as-isolated sample of P5A-NiSOD is confirmed by its EPR spectrum, shown in **Figure 3**. Both the variant and WT enzymes reveal rhombic S = ½ signals that are consistent with low-spin d^7 Ni(III) centers with d^1_{z2} ground states and have similar g-values (P5A-NiSOD: $g_x = 2.36$, $g_y = 2.28$, and $g_z = 2.06$; WT-NiSOD: $g_x = 2.30$, $g_y = 2.22$, $g_z = 2.01$[4, 5]). Both samples show well-resolved ^{14}N-hyperfine (I = 1) on the high-field feature with similar coupling constants (P5A-NiSOD: A_{zz} = 25.9 G; WT-NiSOD: A_{zz} = 24.9 G) that was previously assigned to the apically coordinated His1 imidazole N-donor in the case of WT-NiSOD[4, 5]. By analogy, the P5A-NiSOD Ni(III) center also features apical coordination of the His1 imidazole ligand. Additionally, P5A-NiSOD reveals partially resolved N-hyperfine on the g_y feature (A_{yy} =

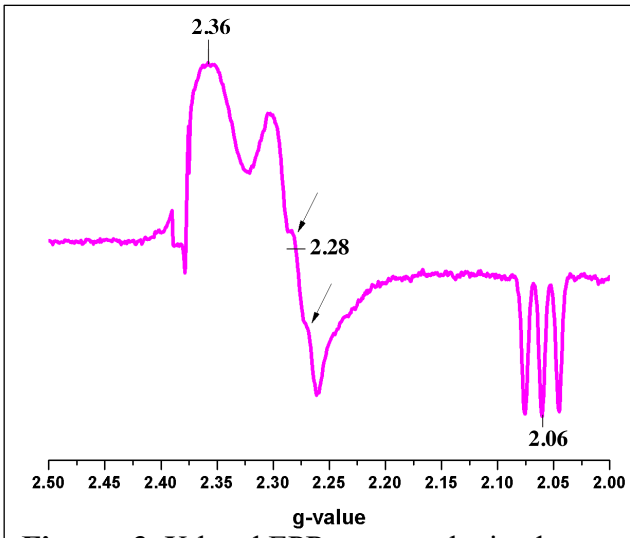

Figures 3. X-band EPR spectra obtained at 77K for as-isolated sample of P5A-NiSOD. The arrows show the partially resolved hyperfine features (A_{yy}= 8.8 G) on the g_y tensor of P5A-NiSOD.

8.8 G) that is not resolved in WT-NiSOD, but is similar to the hyperfine observed on the g_y feature for WT-NiSOD treated with azide, where azide binds to the protein without coordinating to the Ni(III) center[4].

Spin integration of the P5A-NiSOD signal indicates that 40% of the Ni is Ni(III) in the as-isolated sample. This value can be compared with 50% for as-isolated WT-NiSOD, where it has been demonstrated that the remaining Ni(II) cannot be oxidized, even by strong oxidants[6].

3.4 X-ray Absorption Spectroscopy

In contrast to the EPR and electronic absorption spectroscopic techniques, which are dominated by the Ni(III) in the as-isolated sample, XAS sees all the Ni and is therefore dominated by the majority Ni(II) fraction in the as-isolated P5A-NiSOD. Nonetheless, the mixture of Ni sites in the sample complicates the analysis of the data. The average structure of the nickel binding site of as-isolated P5A-NiSOD was examined using Ni K-edge XAS and the results are summarized in **Figure 4** and **Table 1.** Comparison of the XANES spectra for as-isolated P5A-NiSOD and as-isolated WT-NiSOD (**Figure 4A**) reveals that the average structures of the Ni sites have been perturbed in the variant relative to those in the as-isolated WT-NiSOD enzyme. As-isolated WT-NiSOD shows a small peak near 8331 eV that is associated with 1s→3d electronic transition (Peak area = 0.035± 0.009 eV^2) and a broad shoulder centered around 8336 eV associated with a 1s→$4p_z$ transition which is consistent with a 5-coordinate pyramidal Ni-complex or with the known 50/50 mixture of five- and four-coordinate species in this sample[5, 15, 20]. As-isolated P5A-NiSOD lacks the 1s→$4p_z$ transition at 8336 eV and only shows the 1s→3d peak at 8331.15 eV with a peak area of 0.031 (±0.001) eV^2, which is consistent with a six-coordinate Ni-site[20, 21]. Furthermore,

as compared to the as-isolated WT-NiSOD, the XANES data of the as-isolated P5A-NiSOD variant features an increase in the white line region (0-50 eV above the edge) that is indicative of an increase in the ratio of N/O- to S- donors[21].

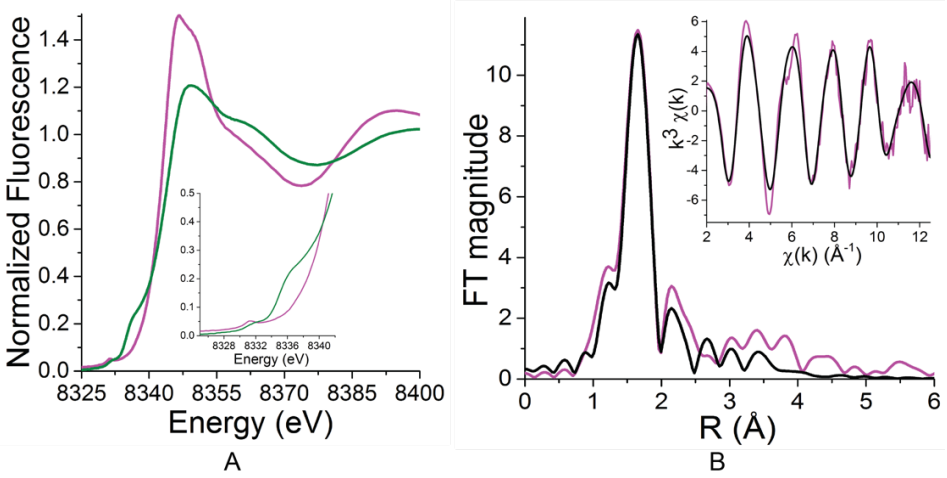

Figure 4: A. Comparison of normalized Ni K-edge XANES region of as-isolated P5A-NiSOD (magenta) and as-isolated WT-NiSOD (green); the inset shows the pre-edge region**. B.** Fourier transformed EXAFS data uncorrected for phase shifts of as-isolated P5A-NiSOD (magenta) and best fit (3.6 N/O (2.07 Å), 0.4 Imidazole (2.06 Å), 1 S (2.37 Å), 1S (2.56 Å); black, k = 2 - 12.5 Å) from Table 1. Insert: Corresponding k^3-weighted unfiltered EXAFS data (magenta) and best fit.

The Ni K-edge EXAFS spectrum of as-isolated P5A-NiSOD and the calculated spectrum for the best fit model are shown in **Figure 4B** and provides evidence for the inclusion of S-scattering atoms in the primary coordination sphere of the Ni center. The best models involving one- and two-shells of scattering atoms are compared with the best fit models in **Table 1**. Other models that were fit to the data are summarized in **Table SI-1**. The only models with acceptable R-factor (< 5%) are found for six-coordinate complexes (in agreement with the XANES analysis) where the two S-scattering atoms are split into two shells, one shell at 2.3 Å and another at 2.6 Å. The 0.3 Å difference in these distances is above the calculated resolution of the data set (0.15 Å). Taken at face value, these distances are more typical of six-coordinate (and therefore high-spin, S= 1) Ni(II) centers[22]. However, it is unclear if the split shell results from the combination of

Ni(III) and Ni(II) centers in the sample. Support for the latter is found in fits where one of the N/O-donors is modeled as a rigid imidazole ring with one adjustable distance (Ni-N). Inclusion of one imidazole improves the overall fit but leads to an unacceptable negative value of σ^2 for the remaining N/O-donors. Adoption of a fractional imidazole ligand (0.4), as determined by EPR integration of the Ni(III) signal, leads to the overall best fit of the data.

Table 1: Best EXAFS fits for as-isolated P5A-NiSOD.

Shell	r (Å)	σ^2 (x10^{-3} Å^{-2})	ΔE_0	% R-factor
6 N/O	2.09(1)	3.7(5)	2(1)	7.2
3 N/O	2.06(1)	0.0(1.7)		
3 N/O	2.16(2)	1(2)	2(1)	6.6
5 N/O	2.09(1)	2.0(1)		
1 S	2.50(2)	20(17)*	2(2)	7.6
5 N/O	2.08(1)	3(1)		
1 Im	2.08(4)	3(5)	2(1)	5.8
4 N/O	**2.07(1)**	**0.5(6)**		
1 S	**2.33(3)**	**1(2)**	**1(1)**	**4.9**
1 S	**2.56(4)**	**2(2)**		
3 N/O	2.07(0)	neg		
1 Im	2.06(5)	4(5)		
1 S	2.35(2)	1(2)		
1 S	2.57(2)	3(2)	1(1)	3.6
3.6 N/O	**2.07(0)**	**0.1(7)**		
0.4 Im	**2.06(5)**	**4(5)**		
1 S	**2.37(2)**	**2(2)**		
1 S	**2.56(2)**	**3(2)**	**1(1)**	**3.5**

*Values in red are outside acceptable ranges; Values in bold represent the best fit model.

3.5 Isothermal Titration Calorimetry

The binding of Ni(II) to apo-WT-NiSOD and apo-P5A-NiSOD was investigated using isothermal titration calorimetry (ITC). In the ITC assays, protein solutions in the sample cell were titrated with a Ni(II) solution. In all cases, the titrations result in negative peaks following Ni(II) additions, indicative of exothermic reactions (**Figure 5, A-C**). **Table 2** reports the binding constants (k_d) for each process, as well as the stoichiometry (N) and the thermodynamic parameters ΔH and ΔS.

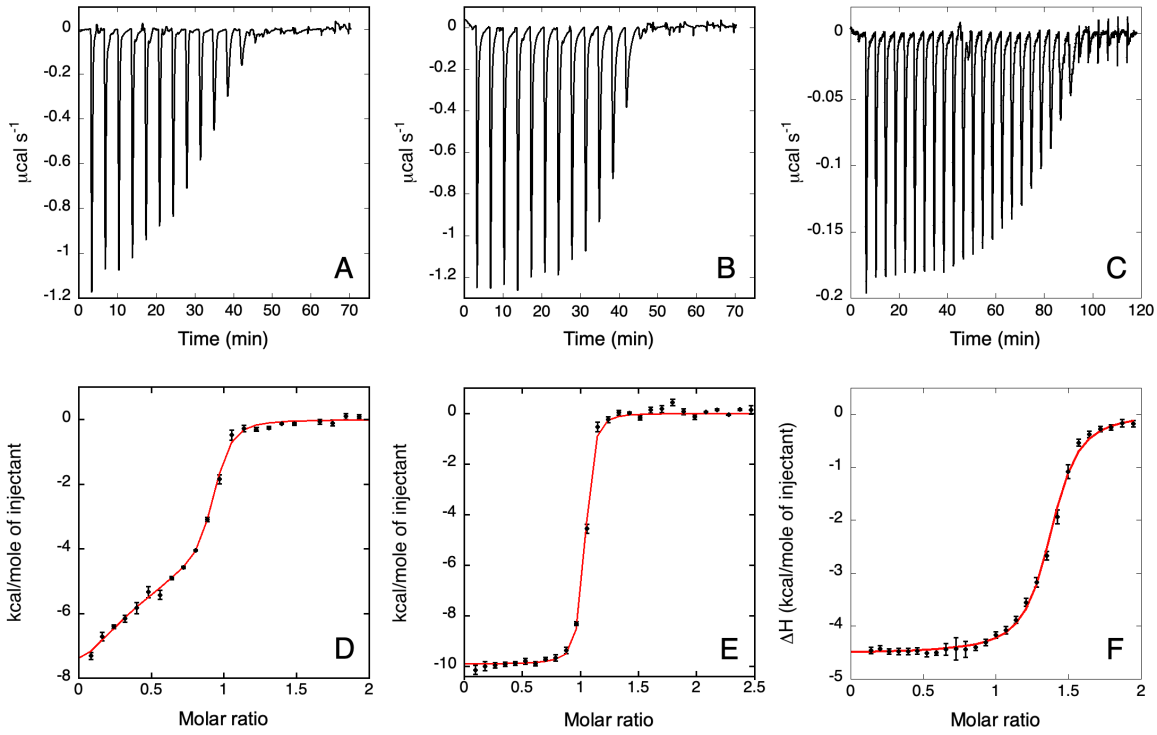

Figure 5. Titrations of apo-WT-NiSOD at 25 °C (A, D) and 35 °C (B, E), and apo-P5A-NiSOD at 25 °C (C, F) followed with ITC. The upper panels show the thermograms, while the lower panels the binding isotherms generated by the integrated heat data (filled circles), and the best fits obtained using the binding models discussed in the text (solid red lines).

For WT-SOD, the shape of the binding isotherm resulting from the integration of the heat peaks for the titration at 25° showed two different slopes (**Figure 5, D**), indicative of two binding events in different sites, prompting the application of a binding model involving two sets of sites for calorimetric data fitting. The first binding event occurs with high affinity in the nanomolar

range, and shows a stoichiometry of N = 0.38(3), suggesting that only a fraction of the protein monomers is involved in this process. A subsequent lower-affinity process occurs in the sub-micromolar range and shows a stoichiometry of N = 0.68(6). The two processes sum to a stoichiometry of 1.06.

Table 2. Thermodynamic data from the ITC study. All the values are given as average and standard deviations of a triplicate experiment. (The values given for ΔH and ΔS are apparent and include contributions not only from metal binding but also from associated events such as protonation/deprotonation of the amino acid residues involved in the binding and consequent change in the buffer ionization state.)

Sample	N	K_d (nM)	ΔH (kcal mol^{-1})	ΔS (cal $mol^{-1}K^{-1}$)	-TΔS (kcal mol^{-1})	ΔG (kcal mol^{-1})
WT-SOD, 25 °C	0.38 ± 0.03 0.68 ± 0.06	25 ± 20 250 ± 60	-9 ± 1 -4.10 ± 0.08	+4 ± 7 +16 ± 3	-0.9 ± 2 -4.8 ± 0.9	-10.4 ± 0.8 -9.00 ± 0.02
WT-SOD, 35 °C	1.06 ± 0.05	33 ± 7	-9.3 ± 0.4	+4 ± 1	-1.2 ± 0.2	-10.5 ± 0.2
P5A-SOD, 25 °C	1.4 ± 0.1	60 ± 20	-4.2 ± 0.3	+19 ± 1	-5.7 ± 0.3	-10.0 ± 0.3

A plausible interpretation of this binding profile is that two different protein conformers are present in solution and contribute to these two separate events, such as might occur if Pro5 was present in both *cis*- and *trans*-conformations. To test this hypothesis, the experiment was repeated at 35 °C, in order to shift the equilibrium between the two conformers toward the less favored *cis*-conformation at higher temperature. The shape of the binding isotherm obtained at 35° shows only a single inflection point, and a fit (**Figure 5, E**) could be achieved using a one site model with a stoichiometry of 1.06(5). The thermodynamic parameters obtained at 35° are indistinguishable from the higher-affinity binding site determined at 25° and indicate that all of the protein is involved in the higher-affinity Ni-binding event at 35 °C.

In contrast to the apo-WT-NiSOD protein, the shape of the P5A-SOD binding isotherm obtained at 25° (**Figure 5, C-F**) showed only a single inflection point, indicative of only one

binding process, and prompted the application of a binding model that involves a single set of sites for the data fitting. The results of the analysis indicate that one Ni(II) ion binds to each P5A-SOD monomer with a lower affinity than observed for the high-affinity site in apo-WT-SOD, and with thermodynamic parameters (ΔH and ΔS) that more closely resemble those of the lower affinity site in apo-WT-NiSOD, suggesting that the high-affinity *cis*-conformation is not present for the apo-P5A-NiSOD sample.

Nickel incorporation into apo-WT-NiSOD is accompanied by oxidation of 50% of the Ni(II) bound to Ni(III) [6]. To rule out spontaneous oxidation of Ni(II) to Ni(III) as a reason for the observation of two binding events, the titration of apo-WT-NiSOD was repeated in buffer containing sulfite. Although this introduced some baseline drift over the course of the titration (likely due to oxidation of sulfite over time), the binding isotherm is not affected by the presence of sulfite (see supporting information **Table SI-3** and **Figure SI-2**) indicating that oxidation is not responsible for the two binding events. This result is also consistent with the lack of a second binding event in the binding isotherm obtained for apo-P5A-NiSOD, which also undergoes spontaneous nickel oxidation to a similar extent upon incorporation of Ni(II) in air (*vide supra*).

3.6 Computational Chemistry

The energies were calculated for the Ni-hook peptide (the first 8 residues of NiSOD from *S. coelicolor*) in the apo-WT-NiSOD, apo-P5A-NiSOD, WT-NiSOD, and P5A-NiSOD forms and are reported in **Table 3.** These values were then used to calculate the energy of the reaction:

According to these calculations, the reaction above is uphill by 6.85 kJ/mol, indicating that the variant protein with *cis*-Ala is less stable than the WT protein with *cis*-Pro.

Table 3. Calculated Energies (a.u.)

Apo-WT-NiSOD	Apo-P5A-NiSOD	WT-NiSOD	P5A-NiSOD
-3498.38733	-3420.98876	-5004.16185	-4926.76067

4. Discussion

Double integration of the first derivative EPR signal observed for as-isolated P5A-NiSOD shows that the amount of Ni(III) present in the as-isolated P5A-NiSOD is a significant fraction of the total nickel present (40%). The fact that the variant is able to support formation of a Ni(III) complex nearly as well as the WT-NiSOD is consistent with the results obtained on model peptides[11]. Another study found that substitution of Pro by Gly in a model peptide led to the formation of a dimeric species attributed to the inability of the variant to wrap around the Ni center[7]. Given that P5A-NiSOD can access the Ni(III) oxidation state in air, it is not surprising that the enzyme is an active SOD, and the modest decrease in k_{cat} from the WT-NiSOD likely reflects a slightly less-favorable Ni(II/III) redox potential in the variant[12]. NiSOD variants that exhibit Ni(III) EPR signals in as-isolated (air-oxidized) samples are invariably active enzymes and exhibit catalytic rate constants that roughly correlate with the

amount of Ni(III) present in the samples (*i.e.,* Ni(II/III) redox potential) (**Figure 6; Table SI-2**). The graph shows an approximately linear relationship between the amount of Ni(III) present in air-oxidized, as-isolated samples, and SOD activity up to the 50% Ni(III) found in WT-NiSOD[6]. This indicates that alteration of the Ni(II/III) redox couple, and thus the rate of formation of Ni(III), may be the dominant factor leading to loss of activity in these variants, with the exception of H1A-NiSOD, which does not show a slow oxidation half-reaction but has a multistep process leading to reduction of Ni(III) that competes with catalysis, rather than establishing a steady state ratio of Ni(II):Ni(III)[15]. The fact that WT- and Y62F (an amino acid variation remote from the active site) lie off the line for the other variants likely shows that mutations also lead to protein alterations that affect the activity in smaller ways, but are optimized for WT-NiSOD.

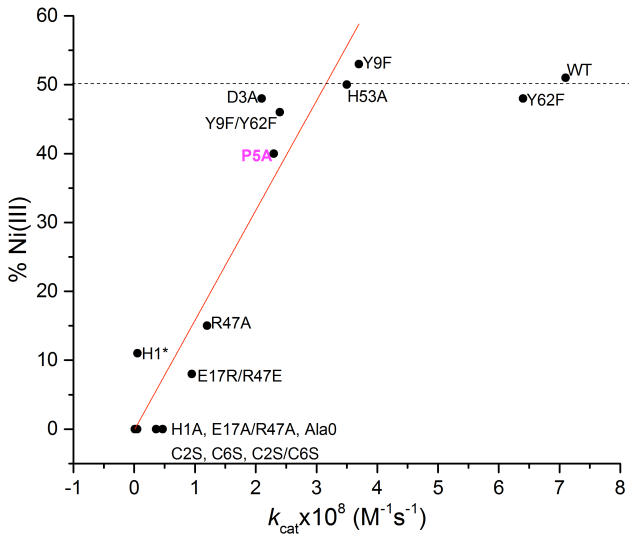

Figure 6. Relationship between the amount of Ni(III) observed in 'air oxidized' as-isolated samples and k_{cat} observed at pH 7.5 (see Table SI-2 for values).The red line represents a least-squares fit to the data excluding Y62F- and WT NiSOD; y = a + bx, where a = -0.18 and b = 15.9, and R = 0.89.

The electronic absorption and EPR spectral characterizations of the as-isolated P5A-NiSOD variant are consistent with the existence of a very similar Ni(III) center to the pyramidal site found in WT-NiSOD[5], which features basal coordination of the His1 N-terminal amine, the Cys2 amidate N-donor, and thiolates from Cys2 and Cys6 (**Figure 1**). That the EPR spectrum obtained from the variant is very similar to that of WT-NiSOD, and is similar to results obtained

on model peptides featuring the same amino acid substitution[11]. The hyperfine on the g_z feature demonstrates apical coordination of the His1 imidazole, as in the WT Ni(III) structure[5]. EXAFS analysis of the as-isolated mixture is consistent with the presence of the Cys2 and Cys6 S-donor ligands, but also reveals considerable structural perturbation from the as-isolated WT-NiSOD structure in that the best fit model of the average structure is six-coordinate and features an additional N/O-donor. Although six-coordinate, low-spin Ni(III) complexes exhibiting EPR signals consistent with S = ½ centers and a $d_{z^2}^1$ electronic configuration are known [23, 24], the EPR signals are generally more axial and such a structural perturbation in the NiSOD site would be expected to lead to distinct EPR parameters, as well as to a change in the energy of S → Ni(III) LMCT that is also not observed. Given the similarity of the Ni(III) site in as-isolated P5A-NiSOD to the WT-NiSOD Ni(III) pyramidal structure, the difference in the EXAFS data likely lies with the reduced Ni(II) site. One possibility is that the Ni(II) site in P5A-NiSOD retains the His1 imidazole and coordinates a water molecule in the remaining axial site. This change in the fairly solvent-exposed Ni site might be produced by the expansion of the Ni-hook motif due to the substitution of *cis*-Pro5 by *cis*-Ala (*vide infra*). Alternatively, the expansion of the Ni-hook could lead to a six-coordinate Ni(II) complex without an imidazole ligand and featuring two axial water molecules. Such a possibility is supported by the EXAFS model featuring 0.4 imidazole donors, which corresponds to the fraction of Ni(III) in the as-isolated sample and improves the fit over one with a full imidazole donor (**Table 1**)

The presence of a WT-NiSOD Ni(III) site implies that the Ni-hook motif is formed in the P5A-NiSOD variant, likely by trapping a *cis*-Ala in the Ni complex. Several studies show that *cis-trans* isomerization of peptide bonds is important for protein folding processes and have implications in cell signaling, ion channel gating and gene expression[25-28]. The disordered N-

terminal region of NiSOD is reminiscent of intrinsically disordered proteins, which feature a high Pro content[29]. Various macrostates of multidomain proteins are attained due to conformational changes induced by *cis*-*trans* isomerization of proline in Xaa-Pro peptides (where Xaa is any amino acid) [25, 30-33]. The *cis*-*trans* amino acid isomerization in proteins may be viewed as involving two states of the backbone that are separated by a significant energy barrier--high enough to give rise to distinct protein conformations that are in slow exchange[30]. Both the *cis*- and *trans*- isomers of proline (dihedral angle ω (Cα-C-N-Cα), which is 0^o for *cis*- and $\pm 180^o$ for *trans*-isomers) are thermodynamically stable with little difference in their Gibbs free energies (ΔG = 0.5 kcal/mol), but are separated by a large kinetic energy barrier ($\Delta G^{\ddagger}$ = 13 kcal/mol) [34, 35]. These differences are larger for the *cis*- and *trans*- isomers of the non-proline peptides (ΔG = 2.5 kcal/mol; $\Delta G^{\ddagger}$ = ~20 kcal/mol)[36]. Thus, in unfolded proteins, Xaa-Pro peptide bonds occur as an equilibrium mixture of both *cis*- and *trans*- isomer (20-30% *cis*-at room temperature[9, 10]) and can populate in either *trans*- or *cis*- conformations with a relatively higher propensity for the *trans*- isomer in folded proteins. In contrast, non-prolyl peptide bonds in folded proteins exist almost exclusively in the *trans*- conformation, though *cis*-conformations are known (estimated to be 0.02% - 0.05% [35-38]), including for Ala [34, 37, 38]. In carbonic anhydrase, a *cis*- conformation is retained in a Leu-Pro202Ala variant[37]. In WT-NiSOD, the fact that Leu4-Pro5 peptide bond adopts a 100%, energetically less favorable *cis*-conformation indicates a role for the Ni complex in trapping the *cis*-Pro5 isomer from the equilibrium mixture of isomers in the structurally disordered N-terminus of the protein. Similarly, it is possible for the Ni complex to kinetically trap the unfavorable *cis*-conformation in P5A-NiSOD.

Support for this model was obtained from Ni(II)-binding studies carried out on WT- and P5A-NiSOD apo-proteins using ITC. The binding isotherms for apo-WT-NiSOD (**Figure 5**) reveal

two binding events with different k_d values. One plausible interpretation is that this reflects binding of Ni(II) to the N-terminus of the WT-NiSOD population that is in the *cis*-Pro5 configuration (essentially a pre-formed Ni-hook, k_d = 25 nM, N = 0.38) and a process reflecting Ni-induced isomerization of the WT-NiSOD population that is in the *trans* Pro5-configuration and binding to the Ni-hook (k_d = 250 nM, N = 0.68), where the apparent k_d value reflects the combination of thermodynamically favorable Ni(II) binding and unfavorable *trans*- to *cis*-Pro5 isomerization. With respect to Ni(II) binding to the *trans*-isomer followed by isomerization of Pro5, the model is in general agreement with that suggested by Barondeau *et al.*[4].

The overall model relies on the fact that the two Pro isomers are separated by a large kinetic energy barrier (*e.g.,* proline switching). The observation that reproducible ITC results could only be obtained after incubating the samples at the experimental temperature for 1.5 – 2 h is consistent with a need to establish the equilibrium mixture where the components are separated by a high kinetic barrier. If this hypothesis is correct, raising the temperature of the experiment from 25° C to 35° C would be expected to increase the population of the less favorable conformation (*cis*-Pro) corresponding to the higher-affinity binding event. Indeed, when the experiment is carried out at 35° C, only a single process corresponding to the high affinity process observed at 25° is present (**Table 2**). In the case of apo-P5A-NiSOD, ITC reveals a single binding event corresponding most closely to the lower-affinity binding process in WT-NiSOD and reflecting the much lower population of *cis*-Ala5 (so small as to be not detected) in the unstructured N-terminus of the variant. Metal-induced isomerization of non-Pro peptide bonds finds precedent in the *trans*- → *cis*-isomerization of Ala-207–Asp-208 in concanavalin A, which is induced by Mn(II) or Ca(II) binding and leads to the formation of the substrate binding site[39].

That both the WT- and P5A-NiSOD proteins are capable of forming stable Ni complexes that feature Ni-hook motifs with *cis*-conformations for the amino acid in the 5th position, was supported by quantum mechanical calculations of models of pre-formed Ni-hooks featuring *cis*-isomers of Pro5 and Ala5. The stability of the Ni(II) complex of the Ni-hook with *cis*-Ala5 was 1.6 kcal/mol less stable than for the model with *cis*-Pro5. This value is lower than the 5 kcal/mol loss of stability found for the Pro202Ala variant of carbonic anhydrase that was attributed to the less favorable *cis-trans* equilibrium in this enzyme[37].

These results beg the question as to why Pro5 is so highly conserved (though not rigorously conserved) when the P5A variant is still a very active enzyme. This could arise if the rate of Ni-binding and concomitant Pro isomerization were important for some, as yet unknown, reason, where the rate of *cis-/trans*- isomerism would be impacted by the Ala substitution. Alternatively, evolutionary pressures could drive maximization of the overall stability of the active site complex.

5. Conclusions

The work presented establishes the Ni-binding affinity of NiSOD and demonstrates that Pro5 is not essential for formation of the Ni-hook motif that is a feature of the active site. The ITC studies presented suggest a Ni(II)-binding model that incorporates formation of the Ni-hook from a dynamic and disordered N-terminus.

Funding:

This work was partially funded by grants from the NIH (GM-069696 to MJM) and NSF (CHE-1111462 to MJM). SC and BZ acknowledge support from the University of Bologna and from CIRMMP (Consorzio Interuniversitario di Risonanze Magnetiche di Metallo-Proteine).

Acknowledgements

We thank Erik Farquhar (Brookhaven National Laboratory) for x-ray absorption data collection. Use of the Stanford Synchrotron Radiation Lightsource, SLAC National Accelerator Laboratory, is supported by the U.S. Department of Energy, Office of Science, Office of Basic Energy Sciences under Contract No. DE-AC02-76SF00515. The SSRL Structural Molecular Biology Program is supported by the DOE Office of Biological and Environmental Research, and by the National Institutes of Health, National Institute of General Medical Sciences (P30GM133894). The contents of this publication are solely the responsibility of the authors and do not necessarily represent the official views of NIGMS or NIH.

References

[1] Y. Sheng, I.A. Abreu, D.E. Cabelli, M.J. Maroney, A.F. Miller, M. Teixeira, J.S. Valentine, Chem. Rev., vol. 114, 2014, pp. 3854-3918.

[2] J.O. Campecino, M.J. Maroney, in: "The Biological Chemistry of Nickel," vol. 10, Royal Society of Chemistry, Metallobiology Series No. 10, D. Zamble, M R-Z Kozlowski and H. Kozlowsky, Eds., 2017 Ch. 9, pp. 170-199.

[3] J. Wuerges, J.W. Lee, Y.I. Yim, H.S. Yim, S.O. Kang, K. Djinovic Carugo, Proc. Natl. Acad. Sci. U S A, vol. 101, 2004, pp. 8569-8574.

[4] D.P. Barondeau, C.J. Kassmann, C.K. Bruns, J.A. Tainer, E.D. Getzoff, Biochemistry, vol. 43, 2004, pp. 8038-8047.

[5] S.B. Choudhury, J.W. Lee, G. Davidson, Y.I. Yim, K. Bose, M.L. Sharma, S.O. Kang, D.E. Cabelli, M.J. Maroney, Biochemistry, vol. 38, 1999, pp. 3744-3752.

[6] R.W. Herbst, A. Guce, P.A. Bryngelson, K.A. Higgins, K.C. Ryan, D.E. Cabelli, S.C. Garman, M.J. Maroney, Biochemistry, vol. 48, 2009, pp. 3354-3369.

[7] C.L. Dupont, K. Neupane, J. Shearer, B. Palenik, Env. Microbiol., vol. 10, 2008, pp. 1831-1843.

[8] J. Shearer, Acc. Chem. Res., vol. 47, 2014, pp. 2332-2341.

[9] S. Osváth, M. Gruebele, Biophys. J., vol. 85, 2003, pp. 1215-1222.

[10] M.S. Weiss, A. Jabs, R. Hilgenfeld, Nat. Struc. Biol., vol. 5, 1998, pp. 676-676.

[11] N. Lihi, G. Csire, B. Szakács, N.V. May, K. Várnagy, I. Sóvágó, I. Fábián, Inorg. Chem., vol. 58, 2019, pp. 1414-1424.

[12] J.O. Campecino, L.W. Dudycz, D. Tumelty, V. Berg, D.E. Cabelli, M.J. Maroney, J. Am. Chem. Soc., vol. 137, 2015, pp. 9044-9052.

[13] F.J. Kim, H.P. Kim, Y.C. Hah, J.H. Roe, Eur. J. Biochem., vol. 241, 1996, pp. 178-185.

[14] K.C. Ryan, O.E. Johnson, D.E. Cabelli, T.C. Brunold, M.J. Maroney, J. Biol. Inorg. Chemistry, vol. 15, 2010, pp. 795-807.

[15] K.C. Ryan, A.I. Guce, O.E. Johnson, T.C. Brunold, D.E. Cabelli, S.C. Garman, M.J. Maroney, Biochemistry, vol. 54, 2015, pp. 1016-1027.

[16] H.T. Huang, S. Dillon, K.C. Ryan, J.O. Campecino, O.E. Watkins, D.E. Cabelli, T.C. Brunold, M.J. Maroney, Inorg. Chem., vol. 57, 2018, pp. 12521-12535.

[17] S.M. Webb, Physica Scripta, IOP Publishing, 2005, pp. 1011-1014.

[18] S. Keller, C. Vargas, H. Zhao, G. Piszczek, C.A. Brautigam, P. Schuck, Anal. Chem., vol. 84, 2012, pp. 5066-5073.

[19] A.T. Fiedler, P.A. Bryngelson, M.J. Maroney, T.C. Brunold, J. Am. Chem. Soc., vol. 127, 2005, pp. 5449-5462.

[20] G.J. Colpas, M. Kumar, R.O. Day, M.J. Maroney, Inorg. Chem., vol. 29, 1990, pp. 4779-4788.

[21] G.J. Colpas, M.J. Maroney, C. Bagyinka, M. Kumar, W.S. Willis, S.L. Suib, P.K. Mascharak, N. Baidya, Inorg. Chem., vol. 30, 1991, pp. 920-928.

[22] J.S. Iwig, S. Leitch, R.W. Herbst, M.J. Maroney, P.T. Chivers, J. Am. Chem. Soc., vol. 130, 2008, pp. 7592-7606.

[23] H.J. Kruger, R.H. Holm, J. Am. Chem. Soc., vol. 112, 1990, pp. 2955-2963.

[24] E.S. Gore, D.H. Busch, Inorg. Chem., vol. 12, 1973, pp. 1-3.

[25] W.J. Wedemeyer, E. Welker, H.A. Scheraga, Biochemistry, vol. 41, 2002, pp. 14637-14644.

[26] T. Kiefhaber, H.P. Grunert, U. Hahn, F.X. Schmid, Biochemistry, vol. 29, 1990, pp. 6475-6480.

[27] M. Levitt, J. Mol. Biol., vol. 145, 1981, pp. 251-263.

[28] F.X. Schmid, R.L. Baldwin, Proc. Natl. Acad. Sci. U S A, vol. 75, 1978, pp. 4764-4768.

[29] B. Mateos, C. Conrad-Billroth, M. Schiavina, A. Beier, G. Kontaxis, R. Konrat, I.C. Felli, R. Pierattelli, J. Mol. Biol., vol. 432, 2020, pp. 3093-3111.

[30] J. Xia, R.M. Levy, J. Phys. Chem. B, vol. 118, 2014, pp. 4535-4545.

[31] K.P. Lu, G. Finn, T.H. Lee, L.K. Nicholson, Nat. Chem. Biol., vol. 3, 2007, pp. 619-629.

[32] A.H. Andreotti, Biochemistry, vol. 42, 2003, pp. 9515-9524.

[33] C. Dugave, L. Demange, Chem. Rev., vol. 103, 2003, pp. 2475-2532.

[34] D.E. Stewart, A. Sarkar, J.E. Wampler, J. Mol. Biol., vol. 214, 1990, pp. 253-260.

[35] M.W. MacArthur, J.M. Thornton, J. Mol. Biol., vol. 218, 1991, pp. 397-412.

[36] A. Jabs, M.S. Weiss, R. Hilgenfeld, J. Mol. Biol., vol. 286, 1999, pp. 291-304.

[37] N.B. Tweedy, S.K. Nair, S.A. Paterno, C.A. Fierke, D.W. Christianson, Biochemistry, vol. 32, 1993, pp. 10944-10949.

[38] L. Jin, B. Stec, E.R. Kantrowitz, Biochemistry, vol. 39, 2000, pp. 8058-8066.

[39] J. Bouckaert, Y. Dewallef, F. Poortmans, L. Wyns, R. Loris, J. Biol. Chem., vol. 275, 2000, pp. 19778-19787.

[40] A.L. Sessions, D.M. Doughty, P.V. Welander, R.E. Summons, D.K. Newman, Curr. Biol., vol. 19, 2009, pp. R567-574.

[41] F. Robert, M. Chaussidon, Nature, vol. 443, 2006, pp. 969-972.

[42] https://www.cpc.ncep.noaa.gov/products/analysis_monitoring/ensocycle/meansst.gif.

Pro5 is not essential for the formation of 'Ni-Hook' in Nickel Superoxide Dismutase

Priyanka Basak[1], Barbara Zambelli,[2] Diane E. Cabelli[3], Stefano Ciurli[3], Michael J. Maroney[1,4*]

Supporting Information

XAS Data Analysis

Table SI-1. Additional selected fits of P5A-NiSOD EXAFS data.

Table SI-2. Amounts of Ni(III) and k_{cat} in as-isolated NiSOD variants

Table SI-3. Thermodynamic data from the titration of apo-WT-NiSOD in the presence of 10 mM Na_2SO_3.

Figure SI-1. SDS-PAGE and ESI-MS for P5A-NiSOD variant.

Figure SI-2. Titrations of apo-WT-NiSOD at 25 °C in the presence of 10 mM Na_2SO_3.

XAS Data Analysis

Data reduction and analyses were performed according to a previously published procedure for Ni K-edge XAS data[1-4]. Briefly, the XAS data shown for as-isolated P5A-NiSOD is an average of eight scans that were normalized and corrected for background. For normalization and background correction, the K-edge energy of Ni was set to 8340 eV with an R_{bkg} of 1. A Gaussian function was used for fitting the pre-edge range and quadratic polynomial functions with 7-8 spline points were used to fit the post-edge range of +100 to +875 eV relative to E_0. The edge jump was normalized by setting the difference between the corrected pre-edge and post-edge baselines to 1. The EXAFS data were converted to k-space using the relationship $[2m_e (E-E_0)/\hbar^2]^{1/2}$, where m_e is the mass of an electron and ħ is Plank's constant divided by 2π. The k^3-weighted EXAFS data were Fourier-transformed over the k-range 2-12.5 $Å^{-1}$ using a Hanning window and fit in r-space using an S_0 value of 0.9. The r-space data shown in the figures was not corrected for phase shifts. The Artemis software program[5] was used for EXAFS analysis with parameters for scattering atoms generated by FEFF6. Multiple-scattering paths for histidine imidazole were generated as previously described[6]. The EXAFS fitting equation used was:

$$\chi(k) = \sum_i \frac{N_i f_i(k) e^{-2k^2\sigma_i^2}}{kr_i^2} sin\,[2kr_i + \delta_i(k)] \quad (1)$$

where *f(k)* is the scattering amplitude, *δ(k)* is the phase-shift, *N* is the number of neighboring atoms, *r* is the distance to the neighboring atoms, and σ_i^2 is a Debye-Waller factor reflecting the mean square deviation in the distance to the nearest neighbor (thermal and static disorder).

To compare the different models fit to the data set, ifeffit utilizes three goodness of fit parameters: χ^2, reduced χ^2 , and the R-factor. χ^2 is given by equation 2, where N_{idp} is the number

of independent data points, N_ε^2 is the number of uncertainties to minimize, Re(fi) is the real part of EXAFS function and Im(fi) is the imaginary part of the EXAFS fitting function.

$$\chi^2 = \frac{N_{idp}}{N_{\varepsilon 2}}\{[Re(fi)2] + [Im(fi)2]\} \qquad (2)$$

Reduced χ^2 represents the degree of freedom in the fit and is given by equation (3)

$$red.\chi^2 = \frac{\chi^2}{N_{\text{idp}} - N_{\text{var}}} \qquad (3)$$

where N_{var} is the number of refining parameters and N_{var} is the number of adjustable parameters. Additionally, ifeffit calculates the R-factor for the fit, which is given by equation (4) and is scaled to the magnitude of the data making it proportional to χ^2.

$$\text{R} = \frac{\sum_{i=1}^{N}\{[Re(f_i)^2]+[Im(f_i)^2]\}}{\sum_{i=1}^{N}\{[Re(xdata_i)]^2+[Im(xdata_i)]^2\}} \qquad (4)$$

In comparing different models, the R-factor and reduced χ^2 parameter were used to determine the model that was the best fit for the data. The R-factor will generally improve with an increasing number of adjustable parameters, while reduced χ^2 will go through a minimum and then increase, indicating that the model is overfitting the data. The resolution of the data (0.15) was determined by equation (5).

$$\text{Resolution} = \frac{\pi}{2\Delta k} \qquad (5)$$

Table SI-1: Additional selected fits of P5A-NiSOD EXAFS data.

Shell	R (Å)	σ^2 (x10^{-3} Å^{-2})	ΔE_0	R-factor (%)	Red. χ^2
		Single Shell			
4 N/O	2.08(0)	**Fits**	2(1)	12.7	66.3
		1.4(7)			
5 N/O	2.09(0)	2.6(0.6)	2(1)	8.8	46.2
6 N/O	2.09(0)	3.7(5)	2(1)	7.2	37.5
4 S	2.18(1)	0.6(8)	-19(3)	15.6	81.8
5 S	2.18(1)	0.7(8)	-18(3)	14.3	75.0
6 S	2.18(1)	0.1(8)	-18(3)	14.3	74.9
		CN = 4			
2 N/O	2.06(1)	neg			
2 S	2.16(2)	1(3)	(-)6(3)	13.7	81.3
2 N/O	2.04(1)	neg			
1 S	2.29(2)	neg	(-)0(3)	9.9	68.7
1 S	2.48(5)	4(5)			
3 N/O	2.06(1)	neg			
1 S	2.16(2)	1(3)	(-)2(3)	11.8	70.2
		CN=5			
4N/O	2.07(1)	1(1)			
1S	2.30(4)	5(5)	0(3)	9.8	57.9
3N/O	2.06(1)	0.6(1.0)			
2S	2.16(2)	7(2)	(-)3(3)	11.6	69.2
3 N/O	2.06(1)	neg			
1 S	2.32(2)	neg	0(1)	6.7	45.9
1 S	2.54(5)	3(5)			
		CN=6			
5 N/O	2.06(1)	1(0)			
1 N/O	2.16(2)	neg	2(1)	6.3	37.3
5 N/O	2.08(1)	3(1)			
1 Im	2.08(1)	3(5)	2(1)	5.8	34.4
4 N/O	2.06(1)	neg			
2 N/O	2.16(2)	1(3)	2(1)	6.4	38.0

3 N/O	2.06(1)	0.0(1.7)			
3 N/O	2.16(2)	1(2)	2(1)	6.5	38.9
5N/O	2.09(0)	2(0)			
1S	2.50(2)	20(22)	2(2)	7.6	45.0
4 N/O	2.08(1)	2(1)			
1 Im	2.05(4)	2(4)			
1 S	2.39(7)	20(8)	1(2)	6.2	43.2
4 N/O	2.08(1)	2(0)			
2 S	2.39(12)	22(15)	1(3)	9.6	56.8
4 N/O	**2.07(1)**	**0.5(6)**			
1S	**2.33(3)**	**1(2)**			
1S	**2.56(4)**	**2(2)**	**1(1)**	**4.9**	**33.6**
3 N/O	2.07(1)	neg			
1 Im	2.06(3)	4(5)			
1 S	2.35(2)	1(2)			
1 S	2.57(2)	3(2)	1(1)	3.6	29.7
3.6 N/O	**2.07(0)**	**0.1(7)**			
0.4 Im	**2.06(5)**	**4(5)**			
1 S	**2.37(2)**	**2(2)**			
1 S	**2.56(2)**	**3(2)**	**1(1)**	**3.5**	**28.9**

Values in red are outside the normal ranges and bold entries show the best fit(s)

Table SI-2: Amounts of Ni(III) and k_{cat} for NiSOD variants

NiSOD	% Ni(III)	k_{cat} ($M^{-1}s^{-1}$) @ pH 7.5
Recombinant WT[7]	51	7.1×10^8
Y62F[7]	48	6.4×10^8
Y9F[7]	53	3.7×10^8
H53A[8]	50	3.5×10^8
P5A	**40**	**2.5×10^8**
Y9F/Y62F[7]	46	2.4×10^8
D3A[7]	48	2.1×10^8
R47A[2]	15	1.2×10^8
E17R/R47E[2]	8	9.5×10^7
H1A[2][1]	0	4.7×10^7
E17A/R47A[2]	0	3.6×10^7
H1*[3]	11	5.6×10^6
C2S[1]	0	5.0×10^6
C6S[1]	0	3.0×10^6
Ala0[4]	0	1.0×10^6
C2S/C6S[1]	0	1.0×10^6
No protein[2]	--	$\sim 1 \times 10^6$

[1]H1A-NiSOD exhibits formation of a Ni(III) species during catalysis that is unstable, unlike in the WT-enzyme[2].
[2]The rate of bimolecular O_2^- disproportionation at a similar concentration of 1 μM and under identical conditions to the catalyzed reactions.

Table SI-3. Thermodynamic data from the titration of apo-WT-NiSOD at 25° in the presence of 10 mM Na_2SO_3, reported in **Figure SI-2**. (The values given for ΔH and ΔS are apparent and include contributions not only from metal binding but also from associated events such as protonation/deprotonation of the amino acid residues involved in the binding and consequent change in the buffer ionization state.)

N	K_d (nM)	ΔH (kcal mol^{-1})	ΔS (cal $mol^{-1}K^{-1}$)	-TΔS (kcal mol^{-1})	ΔG (kcal mol^{-1})
0.42 ± 0.06 0.59 ± 0.06	25 ± 20 400 ± 80	-6.2 ± 0.4 -4.9 ± 0.4	+14.0 +12.9	- 4.2 -3.8	-10.4 ± 0.8 -8.7 ± 0.2

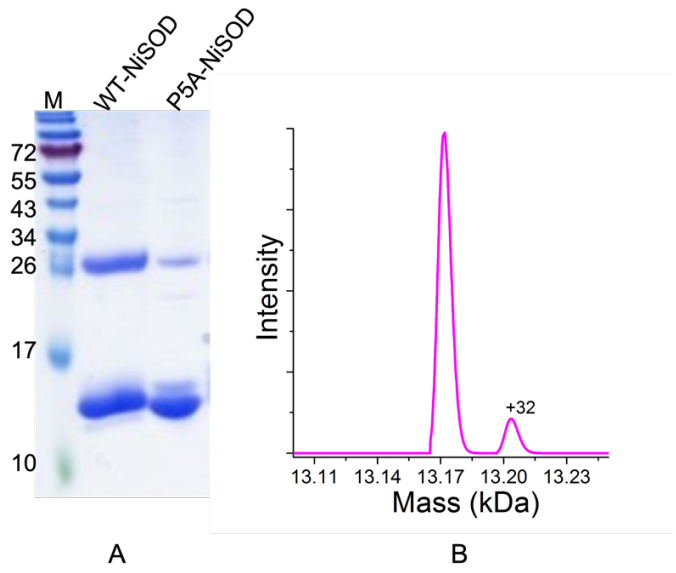

Figure SI-1. **A)** SDS-PAGE showing purified apo-WT-NiSOD and apo-P5A-NiSOD. Higher molecular weights correspond to dimers and are likely due to disulfide formation on exposure to air. **B)** ESI-MS trace of P5A-NiSOD showing 13.17 kDa peak corresponding to P5A-NiSOD monomers. The peak at +32 is attributed to oxidation of cysteine thiols to S-oxygenates upon exposure to air.

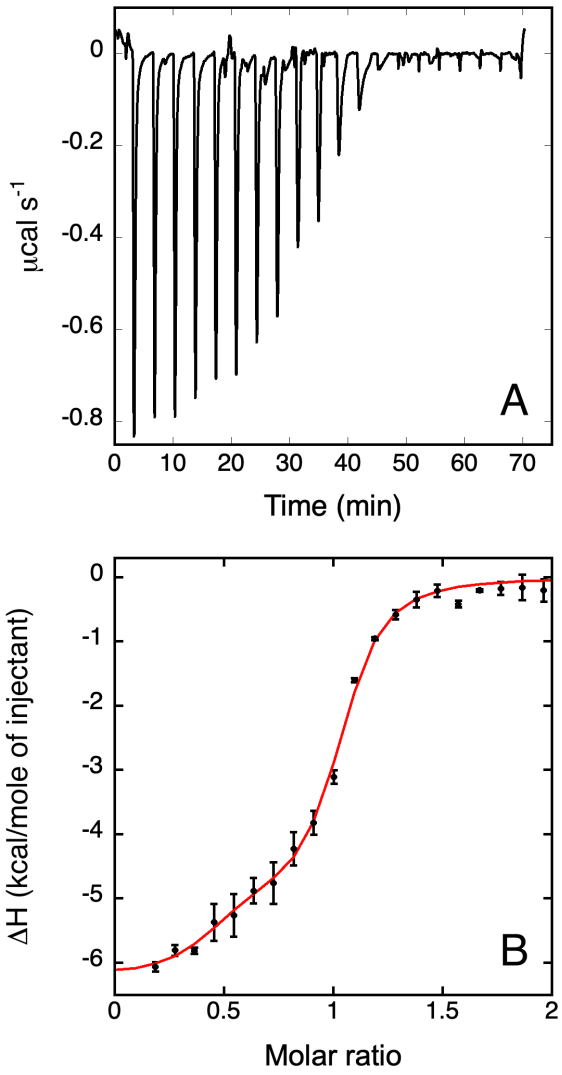

Figure SI-2. Titrations of apo-WT-NiSOD at 25 °C in the presence of 10 mM Na_2SO_3. The upper panel shows the thermogram, while the lower panel shows the binding isotherm generated by the integrated heat data (filled circles), and the best fit obtained using the two site model discussed in the text (solid red lines).

References

[1] K.C. Ryan, O.E. Johnson, D.E. Cabelli, T.C. Brunold, M.J. Maroney, J. Biol. Inorg. Chem., vol. 15, 2010, pp. 795-807.

[2] K.C. Ryan, A.I. Guce, O.E. Johnson, T.C. Brunold, D.E. Cabelli, S.C. Garman, M.J. Maroney, Biochemistry, vol. 54, 2015, pp. 1016-1027.

[3] J.O. Campecino, L.W. Dudycz, D. Tumelty, V. Berg, D.E. Cabelli, M.J. Maroney, J. Am. Chem. Soc., vol. 137, 2015, pp. 9044-9052.

[4] H.T. Huang, S. Dillon, K.C. Ryan, J.O. Campecino, O.E. Watkins, D.E. Cabelli, T.C. Brunold, M.J. Maroney, Inorg. Chem., vol. 57, 2018, pp. 12521-12535.

[5] B. Ravel, M. Newville, J. Synch. Radiat., vol. 12, 2005, pp. 537-541.

[6] H.Q. Hu, R.C. Johnson, D.S. Merrell, M.J. Maroney, Biochemistry, vol. 56, 2017, pp. 1105-1116.

[7] R.W. Herbst, A. Guce, P.A. Bryngelson, K.A. Higgins, K.C. Ryan, D.E. Cabelli, S.C. Garman, M.J. Maroney, Biochemistry, vol. 48, 2009, pp. 3354-3369.

[8] C. Carr, University of Massachusetts Libraries, 2017.